Solid-State and Solution Structure of the Salinomycin−Sodium Complex: Stabilization of Different Conformers for an Ionophore in Different Environments

Erich F. Paulus, Michael Kurz,* Hans Matter, and László Vértesy

Contribution from Hoechst Marion Roussel, Core Research Functions, G865, D-65926 Frankfurt/Main, Germany

Received October 16, 1997

Abstract: The conformation of the ionophore−metal complex between salinomycin and sodium was determined in solid state and in solution using X-ray single-crystal structure analysis and a combined approach of 2D-NMR spectroscopy with restrained simulated annealing calculations. The solution structure of the salinomycin−Na complex was studied in two different solvents (DMSO-d_6 and $CDCl_3$) in order to focus on conformational differences in various molecular environments. The X-ray structure of the complexed salinomycin is characterized by two separate conformers found in the asymmetric unit with a similar coordination of the central sodium ion buried in the interior, hydrophilic region of this ionophore. A quasi-macrocyclic core structure is stabilized by numerous metal−oxygen electrostatic interactions and by an intramolecular head-to-tail hydrogen bond. The NMR structure in $CDCl_3$ is very similar to those two conformations in the solid state, while the structure in DMSO differs significantly. It could be demonstrated that previously published NMR data in $CDCl_3$ do not define a unique conformational state with sufficient accuracy, while this was possible using our own NMR derived datasets discussed herein. For conformer classification and comparison, steric field descriptors based on the CoMFA methodology are used in conjunction with a principal component analysis to uncover the most relevant structural differences between individual salinomycin−Na structures. These studies provided insight into the specific requirements of metal binding for this important polyether ionophore, which could serve as a model system for studying ion transport across biological membranes. Different environments tend to stabilize different conformations of the outer sphere, while the complexation pattern and the geometry of the coordination sphere of the sodium ion remains unaffected.

1. Introduction

Salinomycin[1] (Figure 1) is a member of the class of polyether antibiotics, produced by *Streptomyces albus*, ATCC 21838. Salinomycin, like other polyethers, has ionophoric properties and is known to mediate the transport of various metal ions, especially sodium and potassium across biological membranes.[2] Due to its antibacterial and anticoccidial activity, salinomycin is widely applied as an effective veterinary drug.

Ion channels in membrans have been the subject of intensive studies because of their physiological and pharmacologial signification. However, very little is known about the biologically active conformation of ionophores, when binding and transporting metal ions. Therefore, the determination of the 3D-structure of ionophore metal complexes in different molecular environments is a prerequisite for understanding the mechanism of the transport through biological membranes.

Only one solid-state structure of a *p*-iodophenacyl derivative of salinomycin has been published until now. However, this derivative is not able to form the biologically relevant conformation due to the blocking of the distal carboxyl-group.[3,4] In 1993, the solution structure of the unmodified salinomycin complexed with sodium (salinomycin−Na) has been reported by means of NMR spectroscopy in $CDCl_3$ and molecular dynamics simulations.[5]

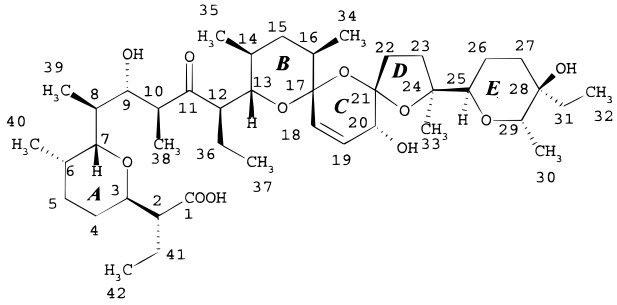

Figure 1. Chemical structure of salinomycin.

In the present study we report the structure of the salinomycin−Na complex in various environments to complement the initial attempts for a full characterization of metal ion binding. We describe the first X-ray structure of the salinomycin−sodium complex obtained from crystals produced by recrystallization from a mixture of water and acetonitrile. The crystals showed in the asymmetric unit two molecules of salinomycin with quite

* To whom the correspondence should be addressed. Tel: ++49-69-305-84394. Fax: ++49-69-305-84401.

(1) Miyazaki, Y.; Shibuya, M.; Sugawara, H.; Kawaguchi, O.; Hirose, C.; Nagatsu, J.; Esumi, S. *J. Antibiot.* **1974**, *28*, 814−821.

(2) Dobler, M. Ionophores and Their Structures; John Wiley & Sons: New York, 1981.

(3) Kinashi, H.; Otake, N.; Yonehara, H.; Sato, S.; Saito, Y. *Tetrahedron Lett.* **1973**, 4955−4958.

(4) Kinashi, H.; Otake, N.; Yonehara, H.; Sato, S.; Saito, Y. *Acta Crystallogr.* **1975**, *B31*, 2411−2415.

(5) Mronga, S.; Müller, G.; Fischer, J.; Riddell, F. *J. Am. Chem. Soc.* **1993**, *115*, 8414−8420.

S0002-7863(97)03607-X CCC: $15.00
Published on Web 08/01/1998

different conformations but a similar way of coordination of the central sodium ion. However, both conformations differ from the published structure in $CDCl_3$, especially at the metal ion coordination site.

Therefore, further studies were undertaken to determine the structure of the salinomycin−Na complex also in solution. Conformational analyses of the ionophore−metal complex were carried out in DMSO-d_6 and $CDCl_3$ solution using a combination of NMR spectroscopy and restrained simulated annealing techniques. As salinomycin is not soluble in water DMSO was used to mimimic the polar environment outside of the biological membrane. The NMR derived experimental data sets include 75 nontrivial distance constraints extracted from 2D ROESY measurements in DMSO-d_6 and 51 distance constraints from $CDCl_3$ solution.

After comparison of 51 distance constraints measured in $CDCl_3$ by Mronga et al.[5] with our own data set, several differences were uncovered. Thus, additional simulated annealing calculations using these published constraints were carried out to unveil, whether identical simulation and analysis protocols generate identical classes of conformers and which dataset was able to better define the low energy conformation. Based on the variety of structural data, finally a detailed comparison will be given to study the structural changes of salinomycin imposed by environmental effects, such as crystal packing or polar versus nonpolar solvents.

2. Methods

2.1. X-ray Structure Analysis. Crystals were obtained by recrystallization from a mixture of water and acetonitrile. A crystal of dimensions 0.7 * 0.35 * 0.2 mm^3 was sealed in a Lindemann-glass capillary. 5501 reflections were used to determine the cell parameters on a computer controlled three circle diffractometer, equipped with a CCD area-detector (SIEMENS). The intensities were measured on the same apparatus [(ω-scanning with stepwidth of 0.2°): Mo−Kα radiation (X-ray generator with a rotating anode: 0.5 × 5 mm^2 focus, 50 kV, 120 mA), 26 943 reflections (ϑ_{min} = 1.47°, ϑ_{max} = 25.67°; −20 < h < 20, −17 < k < 17, −21 < l < 20)], 15 407 of which were unique (R_{int} = 0.0488, R_σ = 0.0913) and were all used for the structure analysis. Direct methods were used for solving the phase problem;[6] refinement of the structure parameters was done by least-squares methods {minimization of $(F_o^2 - F_c^2)^2$;[7] weighting scheme: $w = 1/[\sigma^2(F_o^2) + (0.2139 * P)^2]$, $P = (\max(F_o^2,0) + 2 * F_c^2)/3$, where σ is according to the counting statistics, 1090 parameters}. The coordinates of the H atoms obtained were from a difference Fourier synthesis (S = 0.766, R = 0.1653 (R = 0.0956 for $|F_o| > 4\sigma$, 4746 reflections), R_w = 0.3178, Δ_{max}/esd = 0.002, minimum and maximum peak in the difference map: −0.26 and 0.44 electrons/Å^3). All calculations were done by a DEC 3000/900 AXP with the SHELXS-90, the SHELXTL-PLUS,[8] and SHELXL-93 programs. Further tables of the results are available from the authors. The average estimated standard deviation (esd) of a C−C bond is 0.007, that of an O−C bond 0.006, and that of Na−O bond 0.005 Å. The average esd of bond angles is 0.5° and that of torsion angles 0.6°.

Table 1. ^1H and ^{13}C Chemical Shifts of Salinomycin−Na in DMSO-d_6 at 27 °C

	^1H	^{13}C		^1H	^{13}C
1		181.50	24		87.40
2	2.66	49.68	25	3.41	73.75
3	3.69	75.06	26	2.13(proS)[a] 1.27(proR)[a]	19.31
4	1.76/1.35	19.66	27	1.51(proR)[a] 1.47(proS)[a]	28.70
5	1.79/1.38	26.29	28		69.32
6	1.71	27.40	29	4.00	75.69
7	3.61	70.39	30	1.17	14.45
8	1.30	35.60	31	1.20	31.59
9	4.04	66.79	32	0.83	6.22
10	2.70	48.38	33	1.56	26.81
11		215.33	34	0.65	15.63
12	2.67	54.86	35	0.85	17.33
13	3.56	75.69	36	1.84/1.28	15.72
14	1.67	32.02	37	0.73	12.85
15	1.62(proS)[a] 1.11(proR)[a]	38.14	38	0.74	12.48
16	1.61	39.98	39	0.63	6.69
17		98.31	40	0.86	10.81
18	6.03	122.04	41	1.31/1.15	23.04
19	5.73	130.42	42	0.82	12.36
20	3.99	65.04	9-OH	5.16	
21		105.92	20-OH	4.97	
22	2.12(proR)[a] 1.82(proS)[a]	35.97	28-OH	5.18	
23	1.91(proR)[a] 1.79(proS)[a]	31.88			

[a] Stereospecific assignment is based on homonuclear coupling constants and ROE distance constraints.

2.2. NMR Spectroscopy. All NMR spectra have been recorded on a Bruker DRX 500 at 27 °C using a solution of 20 mg of salinomycin−Na in 0.6 mL of DMSO-d_6 or $CDCl_3$, respectively. The data were processed on Indigo2 workstations (Silicon Graphics) with the XWINNMR software.[9]

Homonuclear 2D-NMR experiments (DQF−COSY,[10] TOCSY,[11] and ROESY[12]) were performed with a spectral width of 8 ppm. These spectra were recorded with 1024 increments in t_1 and 4096 complex data points in t_2. For the ROESY 16 transients were averaged for each t_1 value, for COSY and TOCSY eight transients. Mixing times of 70 or 150 ms were used for TOCSY and ROESY spectra, respectively. Quantitative information on interproton distances for the structure determination was obtained from analyzing ROESY spectra in DMSO-d_6 and $CDCl_3$ with 150 ms mixing time for the spinlock period and a spin lock field of 3.00 kHz. The volume integrals of the individually assigned cross-peaks were converted into distance constraints using the *Isolated Spin Pair Approximation*, the offset effect was taken into account.[13]

For HMQC[14] spectra 1024 increments (16 scans) with 4096 complex data points in t_2 were collected using a sweep width of 8 ppm in the proton and 165 ppm in the carbon dimension. The HMBC[15] spectra were acquired with a sweep width of 8 ppm in the proton and 200 ppm in the carbon dimension. A total of 48 transients were averaged for each of 1024 increments in t_1, and 4096 complex points in t_2 were recorded. A delay of 70 ms was taken for the development of long-range correlations.

(6) Sheldrick, G. M. SHELXS-86, Program for the Solution of Crystal Structures; University of Göttingen: Germany, 1990.
(7) Sheldrick, G. M. SHELXL-93, Program for the Refinement of Crystal Structures; University of Göttingen: Germany, 1993.
(8) Sheldrick, G. M. SHELXTL-PLUS, Release 4.1., An Integrated System for Solving, Refining and Displaying Crystal Structures from Diffraction Data; Siemens Analytical X-ray Instruments Inc.: Madison, WI, 1991.
(9) Bruker XWINNMR; Bruker Analytische Messtechnik GmbH: 1995.
(10) Derome, A.; Williamson, M. *J. Magn. Reson.* **1990**, *88*, 177−185.
(11) Bax A.; Davis, D. G. *J. Magn. Reson.* **1985**, *65*, 355−360.
(12) Bothner-By, A. A.; Stephens, R. L.; Lee, J.; Warren, C. D.; Jeanloz, J. W. *J. Am. Chem. Soc.* **1984**, *106*, 811−813.
(13) Griesinger, C.; Ernst, R. R. *J. Magn. Reson.* **1987**, *75*, 261−271.
(14) Bax, A.; Subramanian, S. *J. Magn. Reson.* **1986**, *67*, 565−569.
(15) Bax, A.; Summers, M. F. *J. Am. Chem. Soc.* **1986**, *108*, 2093−2094.

Table 2. Distance Constraints for Salinomycin−Na Obtained from 500 MHz 2D-ROESY Spectrum in DMSO-d_6 in Comparison with Results Obtained by Averaging Using All Structures from the First Plateau of the *DMSO_1* Simulation[a]

ATOM1	ATOM2	LOWER	UPPER	AV_DIST	AV_VIOL	RMS_VIOL
H2	H7	2.34	2.86	2.19	0.15	0.16
H2	QC42	2.70	4.30	3.28	0.00	0.00
H2	H6	2.70	3.30	3.95	0.65	0.66
H2	H4E	2.52	3.08	3.12	0.07	0.10
H2	H41A	2.61	3.19	2.86	0.06	0.11
H3	H9	3.78	4.62	4.03	0.00	0.00
H3	QC42	2.70	4.30	4.03	0.17	0.22
H3	QC40	3.96	5.84	4.53	0.00	0.00
H3	H41A	2.61	3.19	2.82	0.09	0.13
H7	H9	2.97	3.63	2.93	0.06	0.09
H7	H6	2.25	2.75	2.36	0.00	0.01
H7	H5A	2.52	3.08	2.54	0.04	0.06
H7	H5E	3.78	4.62	3.71	0.07	0.10
H7	H8	3.06	3.74	3.02	0.05	0.07
H7	QC40	3.33	5.07	3.85	0.00	0.00
H7	QC42	4.86	6.94	5.29	0.00	0.01
H7	QC39	2.52	4.08	3.14	0.00	0.00
H7	H20OH	4.59	5.61	5.80	0.20	0.24
H7	H9OH	3.06	3.74	2.39	0.67	0.68
H7	H19	4.59	5.61	5.73	0.15	0.20
H9	H13	2.79	3.41	3.49	0.10	0.13
H9	H8	2.34	2.86	2.43	0.01	0.03
H9	QC33	3.87	5.73	5.00	0.00	0.00
H9	QC35	3.51	5.29	5.95	0.66	0.68
H9	QC38	2.34	3.86	3.18	0.00	0.00
H9	QC39	2.61	4.19	3.76	0.00	0.00
H10	QC33	3.60	5.40	5.48	0.11	0.16
H10	QC37	2.70	4.30	3.71	0.04	0.11
H10	QC39	2.34	3.86	2.97	0.00	0.00
H10	H9OH	3.60	4.40	3.50	0.10	0.13
H12	QC33	3.60	5.40	5.38	0.05	0.10
H12	QC37	2.70	4.30	3.36	0.00	0.00
H12	QC35	2.34	3.86	2.94	0.00	0.00
H12	H14	2.88	3.52	3.09	0.01	0.03
H12	H18	3.60	4.40	4.72	0.32	0.34
H13	H18	1.98	2.42	2.32	0.01	0.02
H13	H19	3.96	4.84	4.17	0.00	0.01
H13	H36B	3.78	4.62	3.74	0.06	0.09
H13	H36A	3.06	3.74	3.97	0.23	0.27
H13	H15A	2.43	2.97	2.93	0.04	0.07
H13	QC35	2.43	3.97	2.93	0.00	0.00
H13	QC37	3.24	4.96	4.90	0.05	0.07
H13	QC39	3.60	5.40	5.66	0.26	0.29
H18	H20	3.42	4.18	3.99	0.00	0.01
H18	H15A	2.25	2.75	2.28	0.02	0.03
H18	QC34	2.70	4.30	3.57	0.00	0.00
H19	H20OH	2.79	3.41	2.64	0.15	0.18
H19	H20	2.52	3.08	2.67	0.00	0.00
H19	QC34	3.24	4.96	4.58	0.00	0.00
H20	H22EX	2.52	3.08	3.10	0.08	0.15
H20	QC34	2.61	4.19	4.17	0.06	0.11
H25	H29	3.96	4.84	3.62	0.34	0.35
H25	H23EN	2.79	3.41	3.39	0.04	0.07
H25	H23EX	3.06	3.74	3.96	0.23	0.25
H25	QC33	2.34	3.86	2.72	0.00	0.00
H25	QC27	2.61	4.09	3.32	0.00	0.00
H25	H26E	2.25	2.75	2.46	0.00	0.00
H25	QC30	2.16	3.64	2.92	0.00	0.00
H25	QC32	4.86	6.94	6.02	0.00	0.00
H25	QC37	4.05	5.95	5.77	0.02	0.07
H25	QC39	4.50	6.50	7.52	1.02	1.02
H25	H20OH	4.23	5.17	4.27	0.06	0.11
H29	QC33	3.60	5.40	5.57	0.17	0.20
H29	QC31	2.97	4.53	3.43	0.02	0.06
H29	QC32	2.43	3.97	3.50	0.10	0.21
H29	H28OH	3.06	3.74	2.59	0.47	0.48
H20OH	QC37	5.22	7.38	7.77	0.41	0.46
H20OH	QC42	3.60	5.40	4.73	0.01	0.03
H20OH	QC30	4.14	6.06	5.10	0.00	0.00
H20OH	QC33	5.58	7.82	5.40	0.19	0.23
H20OH	H22EN	4.32	5.28	3.74	0.58	0.61
H20OH	H23EN	4.05	4.95	4.74	0.02	0.04
H20OH	H26A	2.79	3.41	2.87	0.06	0.09
H28OH	QC32	3.15	3.85	3.17	0.09	0.15
H28OH	H26A	4.05	4.95	3.68	0.37	0.39

[a] LOWER: lower boundary, UPPER: upper boundary including appropriate pseudoatom correction, AV_DIST: averaged distance obtained from acceptable conformers from the *DMSO_1* simulation, AV_VIOL: average distance constraint violation from acceptable conformers from the *DMSO_1* simulation, RMS_VIOL: root-mean-square distance constraints violation from acceptable conformers from the *DMSO_1* simulation.

Table 3. Additional Constraints for *DMSO_1*, *CDCl3_1*, and *CDCl3S_1*

	xray1	xray2	*DMSO_1*[a]	*DMSO_2*	*CDCl3_1*	*CDCl3_2*	*CDCl3S_1*	*CDCl3S_2*
Na-1aO	3.053	3.194	2.195(0.091)	2.115(0.018)	2.143(0.033)	2.077(0.022)	2.258(0.100)	2.087(0.042)
Na-1bO	2.495	2.433	2.099(0.052)	2.059(0.009)	2.076(0.018)	2.075(0.017)	2.102(0.039)	2.079(0.052)
Na-9O	3.081	3.690	3.316(0.150)	3.700(0.721)	2.821(0.180)	2.873(0.245)	2.675(0.187)	4.080(1.599)
Na-11O	2.436	2.356	2.195(0.095)	2.203(0.025)	2.262(0.053)	2.327(0.125)	2.472(0.161)	2.573(0.472)
Na-21O	2.487	2.486	2.206(0.076)	2.144(0.014)	2.216(0.110)	2.190(0.063)	2.334(0.129)	3.596(0.904)
Na-25O	2.415	2.402	2.257(0.138)	2.331(0.177)	2.278(0.112)	2.319(0.211)	2.431(0.173)	5.064(1.934)
1O-28OH	2.833	3.255	2.903(0.172)	3.724(0.610)	2.514(0.068)	3.555(0.824)	2.744(0.303)	4.964(2.188)
1O-9-OH	2.707	2.654	2.576(0.117)	2.822(0.839)	2.548(0.070)	3.230(0.616)	2.828(0.256)	4.872(1.369)

[a] The distances correspond to the average value over all structures of the first plateau for each calculation. The standard deviation is given in parentheses.

2.3. Computational Procedure. All modeling work was performed using the program package SYBYL,[16] version 6.3 on Silicon Graphics workstations. Starting structures were modeled interactively, energy calculations were based on the TRIPOS 6.0 force field[17] including Gasteiger-Marsili charges.[18] All calculations were done on molecules without formal charges. Automation of analysis steps was done using the *Sybyl Programming Language* (SPL).

The first ROE restrained *Simulated Annealing* calculation[19−21] was performed using a set of 75 nontrivial constraints taken from DMSO-d_6. Eight additional distance constraints including close contacts between salinomycin oxygen atoms and the central sodium ion as well as between the distal carboxyl group and 28-OH and 9-OH were added to enhance the convergence rate[22] during simulated annealing, leading to the run *DMSO_1* (see Table 3). For those additional constraints lower bounderies were set to 1.8 Å, upper boundaries to 3.2 Å. In preliminary simulations these distance constraints were found to be redundant. To check the validity of this approach, these additional constraints were disregarded in another run *DMSO_2*. Additionally two simulated annealing runs were performed using 51 distance constraints from NMR measurements in $CDCl_3$ with and without the utilization of the additional distance constraints leading to runs *CDCl3_1* and *CDCl3_2*, respectively. Finally the set of 51 constraints from Mronga et al.[5] was used with and without additional distance constraints (*CDCl3S_1* and *CDCl3S_2*).

A time step of 0.5 fs was used for the integration of Newton's equation of motion[23] for a duration of 750 ps for each simulation. Kinetic energy was included by coupling the entire system to a thermal bath.[24] The dielectric constant was set to 1. The ROE derived distance constraints were applied as a biharmonic constraining function with a force constant of 10 kcal/mol*Å^2. Upper and lower distance limits were set to ±10% of the experimental distances, for nondiastereotopically assigned methylene and methyl protons, 0.9 and 1.0 Å were added to the upper bound. The atomic velocities were applied following a Boltzmann distribution about the center of mass to obtain a starting temperature of 700 K. After simulating for 1.0 ps at this high temperature, the system temperature was stepwise reduced using an exponential function over a 2.0 ps period to reach a final temperature of 200 K. This results in 250 cycles of a 3.0 ps simulated annealing protocol for each simulation, resulting conformers were minimized.

Molecular steric fields as 3D shape descriptor based on the CoMFA method[25,26] were applied to classify all conformers.[27] All superimposed acceptable structures from the maximum RMSD analysis of the simulated annealing calculations plus both X-ray conformers were used as input data set. After the definition of a superposition rule based on an iterative fitting approach[28,29] starting with all heavy-atoms of salinomycin, the steric interaction energies between a probe atom (sp^3-carbon) and each conformer are calculated at surrounding points of a predefined grid (1 Å grid spacing). On the resulting steric fields principal component analyses[30,31] (PCA) were carried out to contract the large number of collinear variables to a few orthogonal "principal conformational properties". The original grid point matrix is approximated by the product of two smaller matrixes, namely scores and loadings.[32] The score matrix now gives a simplified picture of the objects (i.e., salinomycin conformers) represented by a few uncorrelated new variables. The first new coordinate describes the maximum variance among all possible direction, the second one the next largest variation among all directions orthogonal to the first one.

(16) SYBYL Molecular Modelling Package, Version 6.3; Tripos: St. Louis, MO, 1996.

(17) Clark, M.; Cramer III, R. D.; Van Opdenbosch, N. *J. Comput. Chem.* **1989**, *10*, 982−1912.

(18) Gasteiger, J.; Marsili, M. *Tetrahedron* **1980**, *36*, 3219−3228. Details of the implementation are given in: Sybyl 6.2 Theory Manual: Tripos: St. Louis, MO, 1995; p 67.

(19) Nilges, M.; Clore, G. M.; Gronenborn, A. M. *FEBS Lett.* **1988**, *229*, 317−324.

(20) Brünger, A. T.; Adams, P. A.; Rice, L. M. *Structure* **1997**, *5*, 325−336.

(21) A comprehensive review on various molecular dynamics techniques is presented in: van Gunsteren, W. F.; Berendsen, H. J. C. *Angew. Chem., Int. Ed. Engl.* **1990**, *29*, 992−1023.

(22) For a useful application of this strategy using torsion constraints in protein structure refinement, see: Güntert, P. Wüthrich, K. *J. Biomol. NMR* **1991**, *1*, 447−456.

(23) (a) Ryckaert, J. P.; Cicotti, C.; Berendsen, H. J. C. *J. Comput. Phys.* **1977**, *23*, 327−343. (b) van Gunsteren, W. F.; Berendsen, H. J. C. *Mol. Phys.* **1977**, *34*, 1311−1327.

(24) Berendsen, H. J. C.; Postma, J. P. M.; van Gunsteren, W. F.; Di Nola, A.; Haak, J. R. *J. Chem. Phys.* **1984**, *81*, 3684−3690.

(25) Cramer III, R. D.; Patterson, D. E.; Bunce, J. E.; *J. Am. Chem. Soc.* **1988**, *110*, 5959−5967.

(26) *3D-QSAR in Drug Design. Theory, Methods and Applications*; Kubinyi, H., Ed.; ESCOM: Leiden (NL), 1993.

(27) Matter, H.; Szilágyi, L.; Forgó, P.; Marinic, Z.; Klaic, B. *J. Am. Chem. Soc.* **1997**, *119*, 2212−2223.

(28) Nilges, M.; Clore, G. M.; Gronenborn, A. M. *FEBS Lett.* **1987**, *219*, 11−16.

(29) Moyna, G.; Mediwala, S.; Williams, H. J.; Scott, A. I. *J. Chem. Inf. Comput. Sci.* **1996**, *36*, 1224−1227.

(30) (a) Dillon, W. R.; Goldstein, M. *Multivariate Analysis: Methods and Applications*; Wiley: New York, 1984. (b) Malinowski, E. R.; Howery, D.G. *Factor Analysis in Chemistry*; Wiley: New York, 1980. (c) Cramer III, R. D. *J. Am. Chem. Soc.* **1980**, *102*, 1837−1849. (d) Stahle, L.; Wold, S. *Multivariate Data Analysis and Experimental Design in Biomedical Research*. In *Progress in Medicinal Chemistry*; Ellis, G. P., West, G. B., Eds.; Elsevier: 1988; pp 292−338. (e) Wold, S.; Albano, C.; Dunn, W. J., III.; Edlund, U.; Esbensen, K.; Geladi, P.; Hellberg, S.; Johanson, E.; Lindberg, W.; Sjöström, M. In *Chemometrics: Mathematics and Statistics in Chemistry*; Kowalski, B. R., Ed.; NATO, ISI Series C 138, D. Reidel Publ. Co.: Dordrecht, Holland, 1984; pp 17−96.

(31) *SYBYL 6.2, Ligand-Based Design Manual*; TRIPOS, Inc.: St. Louis: MO, 1995; pp 220−225.

(32) Rännar, S.; Lindgren, F.; Geladi, P.; Wold, S. *J. Chemometrics* **1994**, *8*, 111−125.

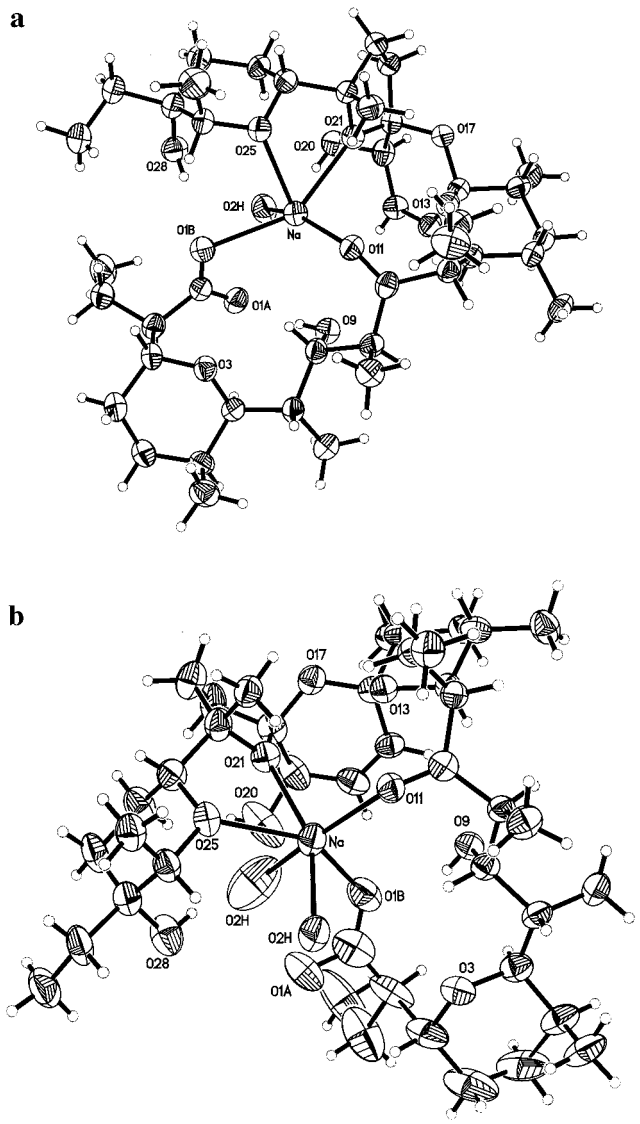

Figure 2. X-ray structures of salinomycin (A: xray1, B: xray2).

3. Results and Discussion

3.1. Solid-State Conformation. The X-ray analysis confirmed the relative and absolute configuration, which was found by Kinashi et al.[3,4] The conformations of the two molecules of the asymmetric unit are slightly different. While the center of the molecule, the tricyclic spiro system, is rigid, the torsion angles at both sides of this system show differences of almost 20°. Conformer 1 (in the following referred to as xray1) is more platelike with one hydrophilic and one hydrophobic side, whereas conformer 2 (xray2) is more spherical (see Figure 2).

The distances between the sodium ion and the oxygens in the first coordination sphere vary from 2.356 to 2.631 Å (see Table 3). In xray1 one water molecule is coordinated to the sodium ion, whereas two water molecules are coordinated in xray2. In the former case a distorted trigonal and in the latter case a distorted tetragonal bipyramid is obtained. Without the water molecules the configuration of sodium in both conformers can be considered as a distorted tetrahedron (Figure 3). None of the oxygens of the three hydroxyl groups is involved in the coordination of the sodium ion which is in contrast to the results of Mronga et al.[5] They found the oxygens in position 9 and 28 to be part of the coordination sphere with a distance between oxygen and sodium of around 2.3 Å.

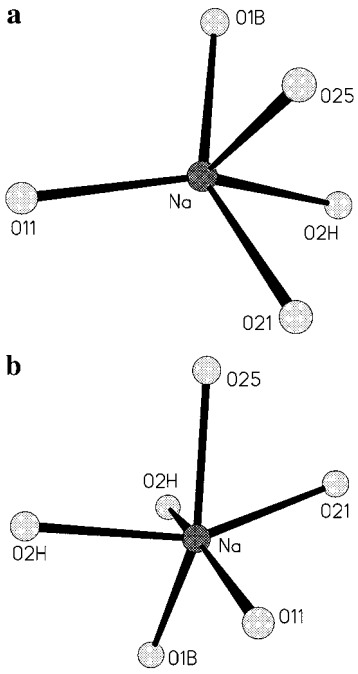

Figure 3. Coordination pattern of the central sodium ion in both solid-state conformers (A: xray1, B: xray2).

In xray2 extremely short distances are observed between the oxygen of a water molecule and three oxygens of salinomycin A: 20-O (2.100 Å), 1a−O (2.421 Å), and 1b−O (2.538 Å). One has to assume that this water oxygen is probably another disordered position of the sodium ion. Least squares refinement calculations show that it is possible to refine a sodium position with a multiplicity of 16.9% and a main position with the multiplicity of 83.1%. The sodium position with the lower multiplicity would be no longer in the center of the hydrophilic pocket resulting in a very distorted trigonal bipyramid configuration.

The intramolecular hydrogen bonds are similar in the two conformers. However, the head to tail bonding (distance between 1a−O/1b−O and 28-OH) is much stronger in xray1 (2.833 Å) than in xray2 (3.251 Å). In xray1 this bonding is performed to the oxygen of the carboxyl group, which is coordinated to sodium, whereas in xray2 the nearest carboxyl oxygen to 28-OH is that one, which is not coordinated to sodium.

All three hydroxyl groups are involved in intramolecular hydrogen bonds. In xray1 9-OH is forming a bifurcated hydrogen bond to 1a−O (2.707 Å) and 11-O (3.047 Å); 28-OH is forming a bifurcated hydrogen bond to 25-O (2.874 Å) and 1b−O (2.833 Å). In xray2 9-OH is correlated with 1b−O (2.654 Å) and 11-O (3.221 Å), while 28-OH is forming hydrogen bonds to 1a−O (3.255 Å) and 25-O (2.910 Å). In both conformers 20-OH is forming an intramolecular hydrogen bond to 21-O (2.850 and 2.768 Å, respectively). The distances show that the bifurcated bonds are usually weaker in xray2 than in xray1. Two water molecules are connecting the two conformers via hydrogen bonds; there are no intermolecular hydrogen bonds between the conformers.

The fully hydrogenated pyran rings have chair conformation. The six-membered ring with one double bond has envelope conformation where 21-C is 0.633 Å (xray1) and 0.557 Å (xray2) out of the plane formed by the other atoms of the ring. The five-membered ring is twisted, atom 21-C is 0.316 (xray1) and 0.212 Å (xray2) out of plane, respectively; atom 22-C is

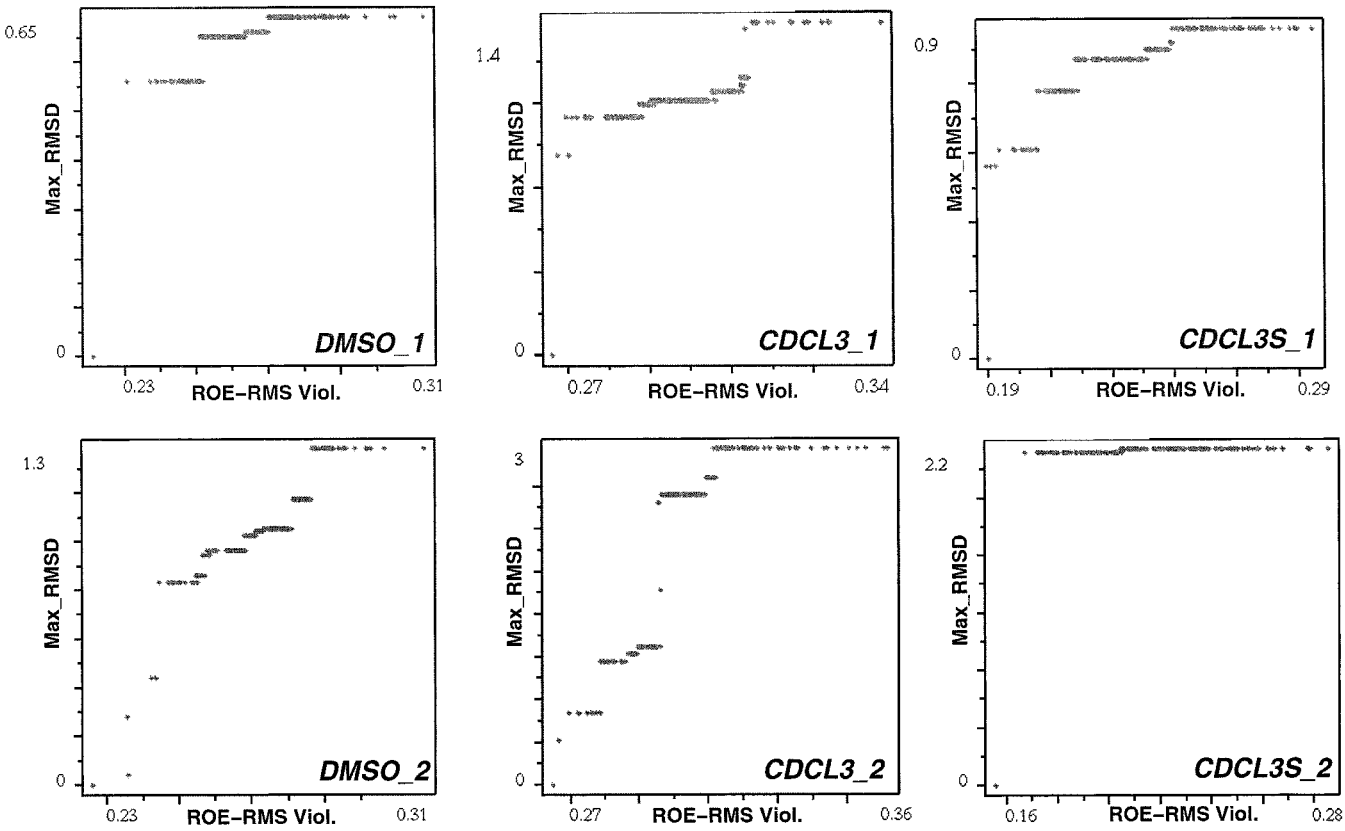

Figure 4. Maximum of the rms deviation between pairs of salinomycin−Na conformers obtained from simulated annealing calculations with a rms ROE violation smaller than a cutoff value as objective criterium for ensemble selection. The sample of structures for rms deviation gets progressively larger with increasing cutoff values for the ROE violation, as plotted on the *x*-axis. On the *y*-axis, the maximum rms deviation values are given. Those plots are shown for all six different simulated annealing calculations; the abbreviations used in this figure directly refer to those runs in the text.

0.225 and 0.387 Å out of the plane of the other ring atoms, respectively.

3.2. NMR Spectroscopy. Resonance assignments of salinomycin−Na in $CDCl_3$ have already been published[5,33,34] and were in accordance with our results. Therefore, only the assignment in DMSO-d_6 based on the analysis of several 2D-NMR-spectra is given in Table 1. As already observed by Mronga et al.,[5] NOESY-spectra of salinomycin−Na suffered from a very low intensity which forced them to use very long mixing times (600 ms). For molecules of this size the ROESY experiment provides a very useful alternative. Using a mixing time of 150 ms and a spinlock field of 3 kHz (at 500 MHz), spectra with high intensities were obtained both in $CDCl_3$ and in DMSO-d_6. The quantitative analysis resulted in 51 and 75 distance constraints in $CDCl_3$ and DMSO-d_6, respectively.

3.2.1. Conformation in DMSO. The structure of salinomycin−Na in DMSO-d_6 solution was determined using 75 interproton distances as constraints in simulated annealing calculations. Acceptable structures were selected based on the maximum pairwise RMSD[35] as objective criterium. Conformers were sorted in ascending order based on the constraint RMS-violations. For each structure the pairwise RMSD to all structures with lower target function values was computed, and the maximum RMSD as a function of the constraint violation value was plotted. The resulting graphs are characterized by steps indicating that additional conformational space becomes available when more violations are tolerated (Figure 4).

For *DMSO_1* (Figure 4, left side, upper panel) where eight additional distance constraints involving close contacts between oxygen atoms and the central sodium ion have been used (see Table 3) the first plateau corresponds to 40 conformers with acceptable constraint violations between 0.22 and 0.26 Å. Conformers representing the second or third plateau form a close structural ensemble similar to the first one. The largest RMS violation from all 250 conformers is only 0.67 Å compared to the conformer with the lowest constraint violation.

The ensemble for *DMSO_1* is displayed in Figure 5. To obtain visually comparable ensembles all plots in Figure 5 show only the best 14 conformers, while numerical analyses were done using the ensembles from the maximum RMSD selection. The comparison between experimental distances and the distances averaged over all structures of the first plateau is given in Table 2. The largest constraint violation of 1.02 Å is observed for the constraint between H25 and the pseudoatom QC39.[36] The corresponding ROE effect was very small leading to a distance constraint between 4.50 and 6.50 Å. For such a small ROE the inaccuracy of the translation into Cartesian distances is not surprising. Four other restraint violations are in the range of 0.58−0.68 Å, while the remaining set is in agreement with the simulations with an averaged restraint violation of 0.120 Å over 75 ROEs and 40 conformers (cf. Table 2).

(33) Anteunis, M. J. O.; Rodios, N. A. *Bull. Soc. Chim. Belg.* **1981**, *90*, 715−735.
(34) Riddell, F. G.; Tompsett S. J. *Tetrahedron* **1991**, *47*, 10109−10118.
(35) Widmer, H.; Widmer, A.; Braun, W. *J. Biomol. NMR* **1993**, *3*, 307−324.

(36) The atom name QC indicates a pseudoatom according to the nomenclature of Wüthrich, K. *NMR of Proteins and Nucleic Acids;* Wiley: New York, 1986.

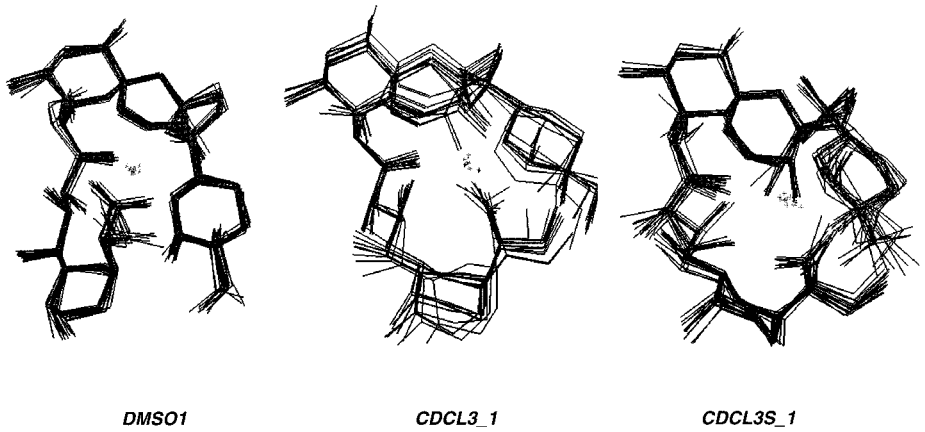

Figure 5. Comparison of the structural ensembles of different salinomycin simulated annealing calculations. The obtained ensembles of 14 best conformers are displayed as superpositions based on the structures with the lowest constraint violations for the set of simulated annealing calculations with additionally constraints involving the sodium atom. Left ensemble: *DMSO_1*; middle ensemble *CDCL3_1*; right ensemble: *CDCL3S_1*. Protons are omitted for clarity.

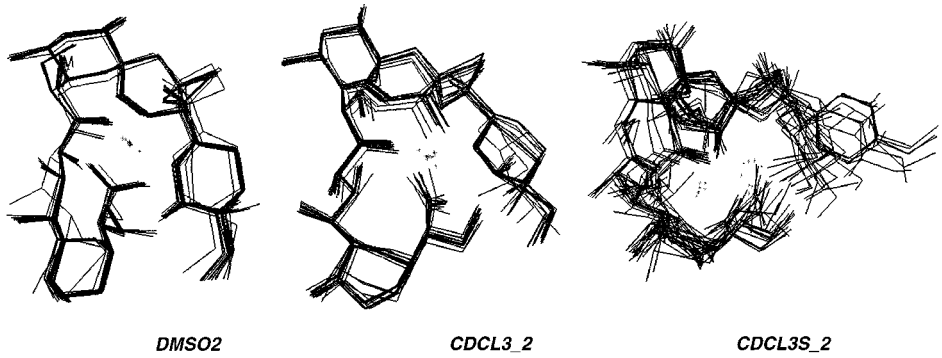

Figure 6. Comparison of the structural ensembles of different salinomycin simulated annealing calculations. The obtained ensembles of 14 best conformers are displayed as superpositions based on the structures with the lowest constraint violations for the simulated annealing calculations without redundant distance constraints. Left ensemble: *DMSO_2*; middle ensemble *CDCL3_2*; right ensemble: *CDCL3S_2*. Protons are omitted for clarity.

The second run *DMSO_2* without additional constraints is leading to very similar results. Taking only the acceptable structures from the first plateau in Figure 4 (lower panel, left) results in an ensemble of 19 structures for analysis (Figure 6, left) without remarkable deviations from the most acceptable conformer except for a single conformer showing some variations of dihedral angles in the linker region connecting rings A and B.

In constrast to *DMSO_1*, those conformers representing higher level plateaus for the *DMSO_2* run in Figure 4 deviate from the well-defined structural ensemble on the first plateau. The rate of convergence is significantly higher applying the additional restraints, but structures with a low deviation from the experimental data are similar in both runs. The largest RMS violation from all 250 conformers from *DMSO_2* is increased from 0.67 to 1.35 Å, while the ROE RMS violations are in the same numerical range (the average restraint violation for 19 structures is 0.119 Å). The same constraint violations are observed as in *DMSO_1* with H25-QC39 showing the highest violation.

While both structures derived from DMSO are similar, they are fundamentally different from solid-state structures. The RMS deviation between xray1 and the DMSO conformer with the lowest restraint violation is 1.82 Å (*DMSO_1*) and 1.95 Å (*DMSO_2*), respectively, while for xray2 RMS deviations of 1.66 and 1.65 Å are obtained.

3.2.2. Conformation in $CDCl_3$. The structure of salinomycin−Na in $CDCl_3$ was determined using 51 distance constraints from 2D ROESY measurements. The first plateau for the run *CDCL3_1* including redundant distance constraints (Figure 4, upper panel, middle) defines a structural ensemble with 14 conformers shown in Figure 5 (middle). Without those constraints, the first observable plateau corresponds to the best 16 structures from the run *CDCL3_2* (Figure 4, lower panel, middle); the ensemble is shown in Figure 6 (middle).

Although more conformational variations in all regions are observed, still a unique structural motif can be identified. For *CDCL3_1* the largest RMS violation from all 250 conformers is 1.3 Å in comparison to the best conformer, while this increases to 3 Å for the simulation without using redundant constraints. The RMS deviation between the best conformers from both runs is 0.86 Å. The averaged restraint violations are 0.127 and 0.124 Å, respectively. In both cases the largest constraint violation of 1.06 A is seen for the distance constraint between H19 and H13, which accounts for the orientation of the first spiro connected bicyclic ring system B and C. The corresponding ROE derived distance was measured as 2.25 Å to 2.75 Å, while the simulations lead to an averaged distance of 3.81 Å. However, the corresponding ROE was found to translate into a much longer distance in the DMSO data set. Here a distance of 3.96−4.84 Å is found, which is in agreement with both simulations. It is interesting to note that this ROE was not present in the data set given in the publication of Mronga.[5] Two other restraints corresponding to protons from the C ring (H19 to H15A and H20 to H23endo) are also violated in both calculations by 0.98 and 0.82 Å, while all other

constraints are fulfilled (see Table 1 of the Supporting Information). Those interactions are not observed in the DMSO data set; only H19 to H15A is reported in the literature—here a longer experimental distance is found in accord with the simulations.

The structures with the lowest restraint violation are more similar to the solid-state structures of salinomycin than the structures in DMSO solution. The RMS deviation between xray1 and both *CDCl3_1* and *CDCL3_2* is 1.25 and 0.75 Å, respectively, while for xray2 RMS deviations of 1.26 and 0.81 Å are obtained, respectively.

Finally, the published constraints in $CDCl_3$ from Mronga et al.[5] were used for two simulated annealing calculations. It was an interesting question to answer, whether identical simulation and analysis protocols would generate identical classes of conformers and which dataset was able to better define the low energy conformations. The first plateau for the run *CDCL3S_1* with published distance constraints including redundant constraints (cf. Figure 2, upper panel, right) corresponds to an ensemble of 16 conformers shown in Figure 3 (right). The structural characteristics are similar to all other salinomycin conformers: a macrocyclic structure closed by the head-to-tail hydrogen bridge and similar interactions between sodium and salinomycin are observed. The ensemble of conformers is defined with a similar quality than the structures based on our own $CDCl_3$ data. The largest RMS violation for all conformers is 1.0 Å in comparison to the conformer with the best constraint violation. The averaged restraint violation is 0.085 Å, because the constraint set includes more restraints involving pseudoatoms with higher tolerated restraint violations. The best structure shows RMS deviations of 1.68 and 1.05 Å to the *CDCL3_1* and *CDCL3_2* conformers, while the RMS deviation to the solid-state structures is 1.47 Å (xray1) and 1.27 Å (xray2), respectively. Again the largest difference is between this ensemble and the structures in DMSO; the RMS deviations are 2.29 and 2.20 Å, respectively.

However, without the redundant constraints it is not possible to identify distinct conformational states as shown in Figure 4 (lower panel, right). Much more conformational variations in all regions are detectable. Thus we selected the best 16 structures based on the ROE RMS violation only. The maximum RMSD value immediately reaches the maximum value of 2.2 Å, indicating that structures with similar ROE RMS violations are very different. This implicates that the literature data set is not able to unambiguously define a unique conformational state with sufficient accuracy. Thus, the observed low averaged restraint violation of 0.077 Å alone does not count for the quality of a structure determination. It has to be pointed out that only for these simulations the use of redundant distance constraints is necessary to obtain an acceptable structural ensemble, while from looking at initial simulations without those constraints, it is difficult to extract redundant information useful for later refinement.

3.3. Principal Component Analysis for Structural Comparison. To analyze structural differences between various conformational ensembles, a principal component analysis (PCA[37]) based on molecular shape descriptors was used. To compute molecular steric fields, all acceptable conformers from six simulated annealing calculations based on the maximum RMSD selection (structures of the first plateau) plus two solid-state structures were superimposed leading to a data set of 123 conformers. The application of a PCA to the molecular steric fields[38] contracts the large number of correlated variables (i.e., steric field energies at discrete gridpoints) to a few, orthogonal *principal conformational properties*.[27] All information describing the conformational variations is contained in the matrix, but it is hidden due to the large number of columns. A PCA now allows for simplification of this data matrix; an informative picture of the underlying structural data can be obtained. Here a total of 13 248 grid points with steric field energies for 123 rows was investigated. Columns with a lower variance than 2.0 kcal/mol were not included in the PCA model, reducing the size of the input data matrix.

The first three orthogonal PCPs in the model (i.e., PCA scores) explain 83% of the overall variance in the data set. The first PCP can explain 54% of the variance, while the second and third components explain 16% and 13%, respectively. The PCA scores can be plotted to reveal the underlying data pattern of the original matrix to identify clusters of objects. Conformers, which are closely related in a score plot have a very similar shape. Thus this plot gives an unambiguous measure on the quality of the resulting conformational ensembles from the simulated annealing calculations, their relationship to other ensembles and the solid-state structures.

The score plots for the PCA model are shown in Figure 7. The three-dimensional score matrix is displayed using projections through the PC1/PC2 plane (Figure 7a) and the PC2/PC3 plane (Figure 7b). Points within these plots represent salinomycin conformers; the distances between points is a direct measure for conformational differences. All conformers from simulations based on the DMSO data set are found in a well-defined cluster at ca. −1/0 in Figure 7a. PC1 differentiates between the conformational ensemble from the *DMSO_1*/*DMSO_2* simulations (ca. −1) and the solid state/$CDCl_3$ based structural ensembles (ca. +1). The second PC2 reveals conformational differences within the set of $CDCl_3$ structures, while the distribution of the DMSO structures is very narrow showing that both sets of distance constraints (with or without redundant constraints) define the same conformational state. From the diameter of this cluster one can conclude that the data set from NMR measurements in DMSO is appropriate to define a single conformation. The second principal component reveals that it is not possible to accurately define a unique conformational state in the *CDCL3_S2* ensemble. The corresponding simulations lead to two (or more) conformational states, well-separated in this principal component, from which one is fundamentally different from all other structures obtained based on $CDCl_3$ data or the solid-state conformers. This one is located at ca. +4 of the second principal component, while all other conformers from various $CDCl_3$ derived simulations are found between −0.5 and 0 on this axis. Both solid-state conformers are located at ca. +0.5 on this second axis. The third and least important principal property PC3 now explains differences between the *CDCL3_1*/*CDCL3_2* ensemble to the *CDCL3S_1/CDCL3S2* ensemble. This principal conformational property shows that both data sets in $CDCl_3$ lead to different conformers. It also shows that both solid-state structures are more similar to conformers from the *CDCL3_1/2* simulations than to those structures obtained using published distance constraints.

3.4. Detailed Analysis of Structural Differences. For this set of 123 conformers from simulated annealing calculations including the two solid-state structures an analysis of dihedral angle distributions was performed to focus on structural

(37) (a) Joliffe, J. *Principal Component Analysis*; Springer: Berlin, 1986. (b) Wold, S.; Esbensen, K.; Geladi, P. *Chemom. Intell. Lab. Syst.* **1987**, *2*, 37−52.

(38) van de Waterbeemd, H., Clementi, S.; Costantino, G.; Carrupt, P. A.; Testa, B. In *3D-QSAR in Drug Design. Theory, Methods and Applications*; Kubinyi, H., Ed.; ESCOM: Leiden, The Netherlands, 1993; pp 697−707.

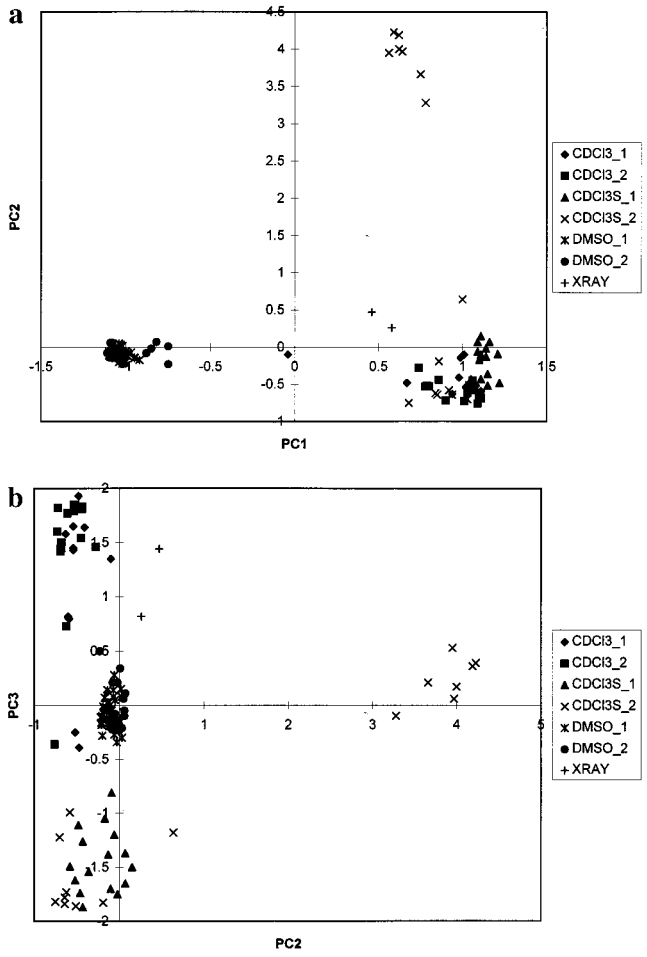

Figure 7. Score plots obtained from the principal component analysis based on molecular shape descriptors and 123 superimposed conformers from various simulated annealing ensembles including solid-state structures. Each score refers to a major principal conformational propertiy (PCP). Different conformational ensembles are indicated by different symbol types, as given as additional legend in both figures. (a) Plot of the first versus the second principal component score. (b) Plot of the second versus the third principal component score.

differences. Due to the formation of the intramolecular head-to-tail hydrogen bond the dihedral angle C1−C2−C3−C4 connecting the terminal carboxyl group to the A ring is locked in a rotameric state between 170° to −155° in all structures. The ethyl group at C2 shows a higher degree of conformational variability in different ensembles. In the *CDCL3_1* and *CDCL3_2* ensemble this torsion is fixed in a +60° orientation, corresponding to both X-ray conformers. This finding is supported by the observed ROEs between H3−QC42 and H2−QC42, which fixes the orientation of the C2−C41 bond. In contrast, the published constraints in $CDCl_3$ and the data from the measurements in DMSO do not lead to a predominant orientation; the rotameric states at −60° and +60° are equally populated. The ROE H3−QC42 is missing in the *CDCL3S* data set, and only H2 shows dipolar interactions with the protons at C42. In DMSO a much weaker interaction between H3−QC42 is observed which is in agreement with both orientations.

The dihedral angle C7−C8−C9−C10 is well-defined at around 160°−185° in *CDCL3_1*, *CDCL3_2*, and the two DMSO ensembles. These values correspond to the X-ray conformers (166.0° and 177.4°). In contrast *CDCL3S_1* and *CDCL3S_2* show higher conformational variability, and values between −180° and −140° (*CDCL3S_1*) and 155° to −170° (*CDCL3S_2*) are observed. The following dihedral angle C8−C9−C10−C11 adopts a narrow range between 160° and 180° for all conformers from the *CDCL3_1* and *CDCL3_2* simulations. In DMSO the averaged value for this torsion has slightly shifted to a narrow range between 180° and −160°. For this torsion both X-ray conformers are very similar to the DMSO derived ensembles (xray1: −167.3°, xray2: −172.0°). For the simulation *CDCL3S_1* different conformations with values between 120° and 160° are found, even more variablility can be observed, when analyzing the ensemble *CDCL3S_2* (dihedral angles between 180° and −80° are found).

The torsion angle C9−C10−C11−C12 varies in *CDCL3_1* and *CDCL3_2* between −130° and −150°, which corresponds to the values found in the two X-ray structures (xray1: −158.7°, xray2: −138.3°). In the DMSO ensembles this dihedral angle is covering a range between −95° and −115°. For the *CDCL3S_1* simulation values between −130° and −170° are found. This torsion appears to be better defined in the unconstrained ensemble from *CDCL3S*_2 (−120° to −150°). A similar difference between the $CDCl_3$ and the DMSO derived ensembles is observed for the torsion angle C10−C11−C12−C13. While for *CDCL3_1* and *CDCL3_2* values between 90° and 105° are found (70°−110° for the *CDCL3S_1* and *CDCL3S_2*), values between 150° and 175° are observed for the DMSO ensembles. Again the $CDCl_3$ ensembles are in agreement with the X-ray conformers, where values of 95.1° and 87.9° are found, respectively. Both torsions reveal a remarkable conformational difference in this linker region between ensembles from measurements in different environments. The final dihedral angle C11−C12−C13−C14 in this linker region is found to adopt similar values for all analyzed ensembles: values between −180° to −160° can be observed in agreement with the crystal conformers (xray1:-165.5°, xray2: −160.5°).

Another conformationally variable linker region is defined by the dihedral angle C23−C24−C25−C26 connecting rings D and E. For the *CDCL3_1*, *CDCL3_2*, and *CDCL3S_1* simulations dihedral angles between 40° and 60° are observed, while from the *CDCL3S_2* simulation values between 40° and 160° are found. For *DMSO_1* values between 10° and 30° were found for this torsion, while *DMSO_2* shows a slightly higher conformational variability with values between 0° and 40°. Again the X-ray data are more similar to the $CDCl_3$ data, values of 54.2° (xray1) and 48.7° (xray2) are found, respectively.

Homonuclear ^3J coupling constants provide additional information about some of these torsion angles. Table 4 contains experimentally determined values observed in DMSO and $CDCl_3$. They are compared to theoretical coupling constants computed using the Karplus equation[39] for each individual structure of the first plateau and subsequently averaged. Those calculated coupling constants are in good agreement with the experimental data. However, large differences and variations of those coupling constants reflected by the reported standard deviation in Table 4 are observed for the two runs using the distance constraints of Mronga et al.[5] In summary all simulations except *CDCL3S_2* result in sufficiently well-defined single conformational states for the linker regions in salinomycin.

This is certainly not true for side-chain regions, as illustrated by the conformational properties of the terminal ethyl group at C28. Three rotameric states (−60, 180, 60°) for the dihedral angle C27−C28−C31−C32 were observed in all ensembles showing the inappropriateness of the NMR data to accurately define a unique conformer. However, the solid-state structures

(39) Karplus, M. J. *J. Chem. Phys.* **1955**, *30*, 11−15.

Table 4. Experimental and Backcalculated Coupling Constants[a]

$J_{H,H}$	Exp_{DMSO}[a]	Exp_{CDCl3}[b]	*DMSO_1*[c]	*DMSO_2*	*CDCl3_1*	*CDCl3_2*	*CDCl3S_1*	*CDCl3S_2*
H6−H7	2.3	2.2	3.56(0.86)	3.61(0.95)	5.21(2.02)	6.72(1.57)	3.52(0.77)	2.79(0.92)
H7−H8	10.1	10.2	10.54(0.30)	9.76(3.04)	10.84(0.05)	10.81(0.04)	10.73(5.16)	7.70(3.94)
H8−H9	1.6	1.6	2.61(0.92)	1.93(0.50)	1.29(0.33)	1.49(0.45)	5.16(2.32)	1.95(1.35)
H9−H10	10.5	10.5	10.56(0.30)	9.47(3.12)	10.72(0.24)	10.87(0.04)	7.71(3.90)	6.97(4.82)
H12−H13	<1.0	<1.0	2.30(0.95)	2.77(0.71)	1.85(0.40)	1.62(0.26)	2.55(0.54)	1.70(0.71)
H13−H14	10.0	10.0	10.47(0.37)	10.69(0.11)	10.89(0.01)	10.90(0.00)	10.83(0.07)	10.78(0.11)

[a] Experimental value in DMSO-d_6. [b] Experimental value in $CDCl_3$. [c] The theoretical coupling constants corresponds to the average value over all structures of the first plateau for each calculation. The standard deviation is given in parentheses. A standard Karplus equation $J = A\cos^2\phi + B\cos\phi + C$ (with $A = 9.4$, $B = -1.1$, and $C = 0.4$) was used to transform the dihedral angle of all structures into the corresponding coupling constants.

show at least two of those three rotamers (xray1: 174.6°, xray2: 63.8°), as there are no structural restrictions imposed on this side chain. Even intermolecular contacts as observed in the solid state are not able to result in a predominant rotamer at this side chain.

A graphical pairwise comparison for the best conformers from the simulated annealing ensembles based on DMSO and $CDCl_3$ derived distance constraints and both solid-state conformers in given in Figure 8a−c.

The metal complexation pattern is very similar in all simulations, except for the *CDCL3S_2* run. A distorted pentagonal pyramid of oxygen atoms is observed within each conformational ensemble involving 1a-O, 1b-O, 11-O, 21-O, and 25-O. For 9-O in none of the cases a close distance to sodium is observed. In the *CDCL3S_2* simulation, 9-O, 21-O, and 25-O are not in close proximity of the central sodium ion leading to an artifical complexation by only three oxygens. The actual distances between various salinomycin oxygen atoms to sodium are summarized in Table 3. When comparing this pattern to the results of the X-ray analysis (values are also given in Table 3), it can be seen that only four oxygens are coordinating the central sodium atom (1a-O, 11-O, 21-O, 25-O). The main difference in the complexation pattern between solid and solution state is the possible interaction of the second oxygen atom of the distal carboxylic group, which is only involved in the NMR derived structures in a complexation. This change is due to a rotation of the plane of the COO− group around the 1-C−2-C bond. Due to the lack of experimentally available information about the actual values for this torsion angle, it cannot be decided, whether this results as artifact from the force-field calculations.

3.5. Comparison with Other Ionophores. To compare the structure of salinomycin−Na with other ionophores a search in the cambridge crystallographic database was performed. In total 26 structures of complexes with different cations were found. Among those complexes only 10 contained sodium (including four structures of monensin.[40] However, the nature of the cation has only minor influence on the coordination pattern and the overall conformation as could be seen from different complexes of monensin with Li^+,[41] Na^+,[40] K^+,[40a,42] and Ag^+.[40a,43] Therefore, all structures were considered for comparison.

Table 5 summarizes the number of oxygens in the coordination sphere. Three different radii (3.0, 3.2, and 3.5 Å, respectively) were chosen to detect all oxygen atoms interacting with the metal ion. The number of oxygens varies between three (lasalocid[44]) and nine (monensin). In most cases the coordination is quite irregular in geometry.

Although there are many structural similarities among the different polyether antibiotic complexes, differences in nature and number of functional groups providing the framework for metal complexation are observed. In all cases tetrahydrofuran rings are involved where the total number is 1 (lasalocid, salinomycin), 2 (alborixin,[45] CP-54,833,[46] dianemycin,[47] grisorixin,[48] lenoromycin,[49] lysocellin[50]), 3 (A-204A,[51] carriomycin,[52] K-41,[53] lonomycin,[54] monensin, nigericin,[55] septamycin[56]), or even 4 (ionomycin[57]). Tetrahydropyran rings are involved in metal binding in alborixin, lasalocid, monensin, nigericin, salinomycin, and septamycin (one ring, respectively), in dianemycin (two), and in lenoromycin (three). A carboxylate carrying one or two coordination partners is present in all polyethers except for lenoromycin and monensin. Other common groups are primary or secondary hydroxyl groups from which mostly two (alborixin, dianemycin, ionomycin, lasalocid, lysocellin, monensin, nigericin) or one (grisorixin, lenoromycin, salinomycin) are taking part in metal complexation. Other typical functional groups are noncyclic aliphatic ethers (A-204A, carriomycin, CP-54,883, grisorixin, K-41, lenoromycin, lono-

(40) (a) Pinkerton, M.; Steinrauf, L. K. *J. Mol. Biol.* **1970**, *49*, 533−546. (b) Ward, D. L.; Wei, K.-T.; Hoogerheide, T. G.; Popov, A. I. *Acta Crystallogr. B* **1978**, *34*, 110−115. (c) Duax, W. L.; Smith, G. D.; Strong, P. D. *J. Am. Chem. Soc.* **1980**, *102*, 6725−6729. (d) Nagatsu, A.; Takahashi, T.; Isomura, M.; Nagai, S.; Ueda, T.; Murakami, N.; Sakakibara, J.; Hatano, K. *Chem. Pharm. Bull.* **1994**, *42*, 2269−2275.

(41) Walba, D. M.; Hermsmeier, M.; Haltiwanger, R. C.; Noordik, J. H. *J. Org. Chem.* **1986**, *51*, 245−247.

(42) Pangborn, W. A.; Duax, W. L.; Langs, D. A. Biophys. *J. Am. Chem. Soc.* **1987**, *109*, 2163−2165.

(43) Agtarap, A.; Chamberlin, J. W.; Pinkerton, M.; Steinrauf, L. *J. Am. Chem. Soc.* **1967**, *89*, 5737−5739.

(44) Aoki, K.; Suh, I.-H.; Nagashima, H.; Uzawa, J.; Yamazaki, H. *J. Am. Chem. Soc.* **1992**, *114*, 5722−5729.

(45) (a) Roey, P. van; Duax, W. L.; Strong, P. D.; Smith, G. D. *Am. Cryst. Assoc., Ser. 2* **1983**, *11*, 24. (b) Roey, P. van; Duax, W. L.; Strong, P. D.; Smith, G. D. *Isr. J. Chem.* **1984**, *24*, 283−289.

(46) Bordner, J.; Watts, P. C., Whipple, E. B. *J. Antibiot.* **1987**, *40*, 1496−1505.

(47) Hauske, J. R.; Kostek, G. *J. Org. Chem.* **1989**, *54*, 3500−3504.

(48) (a) Alléaume, M.; Hickel, D. *Chem. Commun.* **1970**, 1422−1423. (b) Alléaume, M.; Hickel, D. *Chem. Commun.* **1972**, 175−176.

(49) (a) Blount, J. F.; Evans, R. H., Jr.; Liu, C.-M.; Hermann, T.; Westley, J. W. *J. Chem. Soc., Chem. Commun.* **1975**, 853−855. (b) Koyama, H.; Utsumi-Oda, K. *J. Chem. Soc., Perkin Trans. 2* **1977**, 1531−1536.

(50) Koenuma, M.; Kinashi, H.; Otake, N.; Sato, S.; Saito, Y. *Acta Crystallogr. B* **1976**, *32*, 1267−1269.

(51) Jones, N. D.; Chaney, M. O.; Chamberlin, J. W.; Hamill, R. L.; Chen, S. *J. Am. Chem. Soc.* **1973**, *95*, 3399−3400.

(52) Otake, N.; Nakayama, H.; Miyamae, H.; Sato, S.; Saito, Y. *J. Chem. Soc., Chem. Commun.* **1977**, 590−591.

(53) Shiro, M.; Nakai, H.; Nagashima, K.; Tsuji, N. *J. Chem. Soc., Chem. Commun.* **1978**, 682−683.

(54) Otake, N.; Koenuma, M.; Miyamae, H.; Sato, S.; Saito, Y. *Tetrahedron Lett.* **1975**, 4147−4150.

(55) (a) Steinrauf, L. K.; Pinkerton, M.; Chamberlin, J. W. *Biochem. Biophys. Res. Commun.* **1968**, *33*, 29−31. (b) Shiro, M.; Koyama, H. *J. Chem. Soc. B* **1970**, 243−253. (c) Barrans Y.; Alléaume, M.; David, L. *Acta Crystallogr. B* **1980**, *36*, 936−938.

(56) Dirlam, J. P.; Belton, A. M.; Bordner, J.; Cullen, W. P.; Huang, L. H.; Kojima, Y.; Maeda, H.; Nishiyama, S.; Oscarson, J. R.; Ricketts, A. P.; Sakakibara, T.; Tone, J.; Tsukuda, K.; Yamada, M. *J. Antibiot.* **1992**, *45*, 331−340.

(57) Toeplitz, B. K.; Cohen, A. I.; Funke, P. T.; Parker, W. L.; Gougoutas, J. Z. *J. Am. Chem. Soc.* **1979**, *101*, 3344−3353.

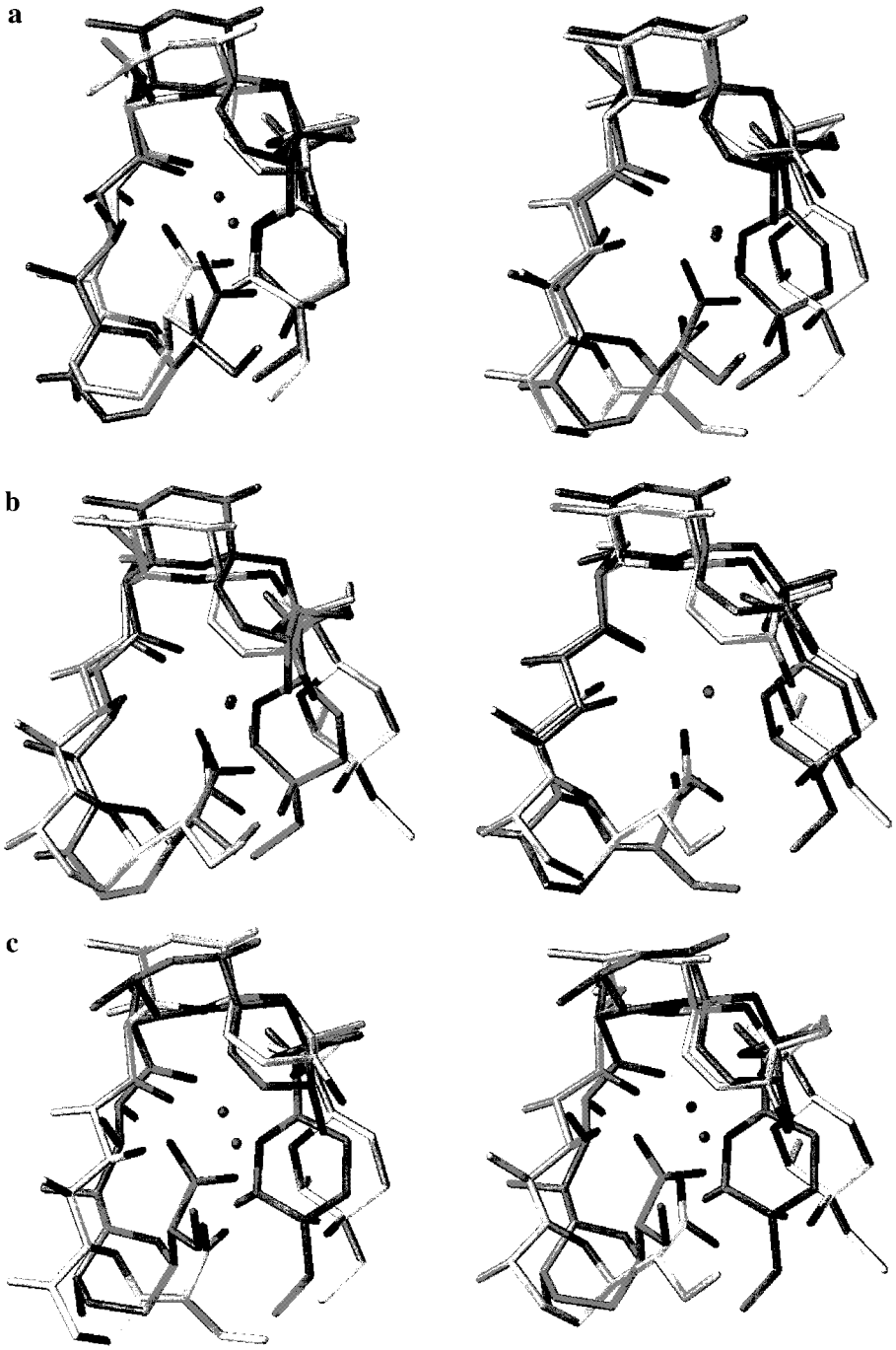

Figure 8. Pairwise comparison for the best conformers from the simulated annealing ensembles based on DMSO and $CDCl_3$ derived distance constraints and both solid-state conformers. For clarity, protons are omitted in all conformer representations. (a) Left: best simulated annealing conformer from the run *DMSO_1* (gray carbons) superimposed on the best simulated annealing conformer from the run *CDCL3_1* (white carbons); right: first solid-state conformer (gray carbons) superimposed on the best simulated annealing conformer from the run *CDCL3_1* (white carbons). (b) Left: second solid-state conformer (gray carbons) superimposed on the best simulated annealing conformer from the run *CDCL3_1* (white carbons); right: second solid-state conformer (gray carbons) superimposed on first solid-state conformer (white carbons). (c) Left: first solid-state conformer (gray carbons) superimposed on the best simulated annealing conformer from the run *DMSO_1* (white carbons); right: second solid-state conformer (gray carbons) superimposed on the best simulated annealing conformer from the run *DMSO_1* (white carbons).

mycin, nigericin, septamycin) and carbonyl groups from keto or ester functions (CP-54,883, grisorixin, ionomycin, lasalocid, lysocellin, monensin, salinomycin).

3.6. Possible Hinge Regions in Salinomycin. The ionophore-mediated transport of metal ions through the membrane includes complex formation, diffusion, and dissociation. While the kinetic of this process has been studied in detail,[58] thermolecular basis of the complex formation and dissociation is still unknown. Different assumptions about the mechanism have been made based on a comparative conformational study of different polyether ionophores[33] or on molecular dynamics calculations,[5] respectively. Anteunis et al.[33] proposed the torsions C9−C10−C11−C12 and C10−C11−C12−C13 together with C23−C24−C25−C26 to be the major hinges when

(58) Riddell, F. G.; Tompsett, S. J. *Biochim. Biophys. Acta* **1990**, *1024*, 193−197.

Table 5. Published X-ray Structures of Polyether Antibiotics[a]

ionophore	cation	no. of oxygens < 3.0 (Å)	no. of oxygens < 3.2 (Å)	no. of oxygens < 3.5 (Å)	lit.
A-204A	Na^+	6	8	8	51
A-204A	Ag^+	6	6	7	51
alborixin	Na^+	6	6	7	45
carriomycin	Tl^+	5	7	8	52
CP-54,883	Na^+	6	6	6	46
dianemycin	Rb^+	3	7	8	47
grisorixin	Na^+	6	6	6	48
ionomycin	Ca^{2+}	7	7	7	57
ionomycin	Tl^+	4	7	7	54
K-41	Na^+	6	6	6	53
lasalocid[b]	Tl^+	3	4, 5	5, 6	44
lenoromycin	Ag^+	7	8	8	49
lonomycin	Tl^+	5	6	8	54
lysocellin	Ag^+	5	6	6	50
monensin	Ag^+	6	7	7	40a, 43
monensin[c]	K^+	6	7	8,9	40a, 42
monensin	Li^+	6	6	7	41
monensin[d]	Na^+	6	7	7	40a−d
nigericin	Ag^+	5	5	6	55a,b
nigericin	Na^+	5	5	5	55c
septamycin	Rb^+	4	7	8	56
salinomycin	Na^+ (xray1)	4	6	6	
salinomycin	Na^+ (xray2)	4	5	5	
salinomycin	Na^+ ($CDCl_3$)	6	6	6	
salinomycin	Na^+ (DMSO)	5	5	5,6	

[a] From Cambridge crystallographic data base. [b] Two structures have been published. [c] Two structures have been published. [d] Four structures have been published.

Table 6. Torsion Angles of Possible Hinge Regions in Salinomycin

torsion	xray1	xray2	*CDCl3_1*[a]	*CDCl3_2*[a]	*DMSO_1*[a]	*DMSO_2*[a]
C6−C7−C8−C9	−172.1	−178.6	−175.5 (6.5)	−171.0 (5.4)	169.6 (5.4)	160.6 (29.8)
C7−C8−C9−C10	166.0	177.4	165.9 (4.3)	168.1 (4.1)	178.5 (4.3)	172.5 (7.8)
C8−C9−C10−C11	−167.3	−172.0	171.3 (5.3)	173.4 (2.0)	−170.7 (5.5)	−159.2 (29.5)
C9−C10−C11−C12	−158.7	−138.3	−138.0 (5.4)	−140.2 (3.6)	−108.1 (6.0)	−103.7 (2.4)
C10−C11−C12−C13	95.1	87.9	94.5 (10.8)	96.5 (4.3)	130.1 (7.1)	133.9 (7.6)
C11−C12−C13−C14	−165.5	−160.5	−173.5 (4.2)	−171.6 (2.1)	−172.5 (6.2)	−178.4 (3.8)
C23−C24−C25−C26	54.2	48.7	55.4 (5.3)	52.6 (6.9)	11.5 (6.9)	0.5 (18.9)

[a] The torsion angles correspond to the average value over all structures of the first plateau for each calculation. The standard deviation is given in parentheses.

salinomycin changes from a closed to an open conformation and vice versa. Performing unconstrained MD simulations with and without the sodium ion Mronga et al.[5] defined the torsions C10−C11−C12−C13 and C6−C7−C8−C9 to be the most important ones, while the torsions C9−C10−C11−C12 and C23−C24−C25−C26 were excluded as possible hinge regions due to their restrictions in flexibility during the calculations. However, none of the assumptions is based on experimental data supporting one of both models.

For the first time, we were able to experimentally determine conformations of salinomycin in different environments and to examine those torsions undergoing the largest conformational changes. Table 6 summarizes the torsion angles possibly involved in the operating mechanism including the two X-ray structures and the results of the calculations in $CDCl_3$ and DMSO. The torsion angles of the two X-ray structures are very similar with the exception of torsion C9−C10−C11−C12 where a difference of 20.4° is observed. Furthermore, no major differences are observed between the structures in $CDCl_3$ and the X-ray structures. In DMSO significantly larger differences are observed for torsions C9−C10−C11−C12, C10−C11−C12−C13, and C23−C24−C25−C26 with respect to the structures in $CDCl_3$ and in the solid state. In contrast, the torsion C6−C7−C8−C9 is well conserved under all experimental conditons used in the present investigation.

Therefore, our results strongly support the model previously proposed by Anteunis et al.[33] It should be pointed out that the torsion angles obtained in the crystal structure of the "open" *p*-iodophenacyl derivative of salinomycin[3,4] give further evidence for the localized hinge regions. While torsions C6−C7−C8−C9 (174.7°), C7−C8−C9−C10 (173.8°), C8−C9−C10−C11 (−172.9), and C11−C12−C13−C14 (176.9°) remain almost uneffected, larger deviations are observed for C9−C10−C11−C12 (−167.9°), C10−C11−C12−C13 (50.9°), and C23−C24−C25−C26 (−66.8°).

4. Conclusion

Structure determination of the salinomycin−sodium complex was carried out in the solid state as well as in two different solvents to analyze the impact of various environments. Salinomycin can be characterized as a molecule with a hydrophilic binding site serving as coordination partner for the central sodium ion and a very hydrophobic surface region, which is exposed to the environment (solvent or membrane). The present study provides insights into structural aspects of metal-ion complexation with a higher degree of confidence with respect to earlier structural analysis.

A quasi-macrocyclic core structure is stabilized by numerous metal−oxygen electrostatic interactions and by an intramolecular head-to-tail hydrogen bond. While the structure in the coordination sphere is very similar in all conformers, the hydrophobic surface region shows significant differences especially in the linker (hinge) regions. Two different structural families

can be distinguished with the DMSO structure being dissimilar to the $CDCl_3$/solid-state structures.

The similarity between the X-ray structures and the conformation in $CDCl_3$ can be regarded as a consequence of the lipophilic environment in both cases: Only intermolecular hydrophobic interactions between different salinomycin molecules are observed in the crystal form, while no intermolecular hydrogen bonds occur. Thus, the structure deduced from experimental data in $CDCl_3$ and in the solid state are more likely to mimic the conformation of the ionophore exposed to a lipophilic membrane.

The quantification and visualization of structural differences between different conformers was possible using principal component analysis on molecular steric fields. A better defined structural ensemble can be obtained with a higher number of diastereotopically assigned protons in the experimental data set. The utilized sets of input distance constraints obtained during the present investigation in DMSO and $CDCl_3$ are sufficient to precisely define the conformations of the salinomycin−sodium complex without the use of additional distance constraints. In contrast, this was not possible using constraint data sets given in the literature.

For the first time, we were able to experimentally determine conformations of salinomycin in different environments and to examine those torsion angles undergoing the largest conformational changes. These torsions are considered to play an important role during complex formation and dissociation. Thus a more detailed picture on metal ion transportation through biological membranes emerges.

Acknowledgment. The authors thank Bernd Beck for purifying and crystallizing the sample of salinomycin.

Supporting Information Available: Tables (T1−T5) with distance constraints and computed averaged distances for salinomycin−Na, atomic coordinates and equivalent isotropic displacement parameters (T6), and anisotropic displacement parameters of the X-ray structures (18 pages, print/PDF). See any current masthead page for ordering information and Web access instructions.

JA973607X